HHS Public Access

Author manuscript

Ann Biomed Eng. Author manuscript; available in PMC 2021 March 01.

Published in final edited form as:

Ann Biomed Eng. 2020 March ; 48(3): 992–1005. doi:10.1007/s10439-019-02279-0.

Evaluation of an Engineered Hybrid Matrix for Bone Regeneration via Endochondral Ossification

Paiyz E. Mikael[1], **Aleksandra A. Golebiowska**[2], **Xiaonan Xin**[3], **David W. Rowe**[3], **Syam P. Nukavarapu**[1,2,4]

[1]Department of Materials Science & Engineering, University of Connecticut, Storrs, CT-06269

[2]Department of Biomedical Engineering, University of Connecticut, Storrs, CT-06269

[3]Center for Regenerative Medicine and Skeletal Development, University of Connecticut Health, Farmington, CT-06032

[4]Department of Orthopaedic Surgery, University of Connecticut Health, Farmington, CT-06032

Abstract

Despite its regenerative ability, long and segmental bone defect repair remains a significant orthopedic challenge. Conventional tissue engineering efforts induce bone formation through intramembranous ossification (IO) which limits vascular formation and leads to poor bone regeneration. To overcome this challenge, a novel hybrid matrix comprised of a load-bearing polymer template and a gel phase is designed and assessed for bone regeneration. Our previous studies developed a synthetic ECM, hyaluronan(HA)-fibrin(FB), that is able to mimic cartilage-mediated bone formation *in vitro*. In this study, the well-characterized HA-FB hydrogel is combined with a biodegradable polymer template to form a hybrid matrix. *In vitro* evaluation of the matrix showed cartilage template formation, cell recruitment and recruited cell osteogenesis, essential stages in endochondral ossification. A transgenic reporter-mouse critical-defect model was used to evaluate the bone healing potential of the hybrid matrix *in vivo*. The results demonstrated host cell recruitment into the hybrid matrix that led to new bone formation and subsequent remodeling of the mineralization. Overall, the study developed and evaluated a novel load-bearing graft system for bone regeneration via endochondral ossification.

1. Introduction

About three million musculoskeletal procedures are performed annually in the United States, half of which involve some type of a bone graft[1], [2]. Autografts and allografts are commonly used for bone grafting. Allografts are often linked to challenges such as disease transmission and immune rejection, while autograft harvesting causes donor-site morbidity

*Corresponding author: Syam P. Nukavarapu, PhD, Associate Professor, Biomedical Engineering, University of Connecticut, 260 Glenbrook Road, Unit 3247, Storrs, Connecticut 06269, Ph: 860-486-6975, syam.nukavarapu@uconn.edu.

with a limited amount of tissue that can be isolated from the patient[3]–[6]. Therefore, tissue engineering is emerging as an alternative strategy for bone defect repair/regeneration.

Biomaterials have had a long history as bone substitutes. Natural and synthetic polymers and their composites with calcium phosphates and hydroxyapatite have been developed into numerous three-dimensional and porous structures[7]–[11]. These developed structures/scaffolds in various types, shapes and configurations are found to support *in vitro* osteogenesis and *in vivo* bone tissue formation[12]–[15]. However, bone formation in these engineered matrices typically go through an intramembranous ossification (IO) process, in which stem/osteoprogenitor cells directly differentiate into osteoblasts. This process often results in bone formation with poor to no vascularization; such a process is not optimal to treat segmental bone defects[16], [17].

Recently, a shift in bone regeneration approach has led many researchers to focus on the endochondral ossification (EO) process, in which MSCs go through the steps of cartilaginous template formation, vascularization and mineralization[18], [19]. Due to the inherent vascularization step, healthy segmental bone regeneration is possible through EO. Zhou et al. studied the potential of an engineered graft seeded with MSCs to form functional bone using a subcutaneous animal model. Both histological and immunohistochemical examination revealed the newly formed bone followed the endochondral pathway[20]. Another study involved pre-differentiated MSCs seeded onto PLGA scaffolds implanted into 5mm and 15mm defect femoral rat models. Eight weeks after implantation the biomechanical strength in the 15mm implant reached 75% that of a normal rat femur. Complete bone union was observed 16 weeks post implantation[21]. Scotti et al. pre-differentiated MSCs seeded onto collagen I meshes for three weeks in chondrogenic media followed by an additional two weeks in hypertrophic media. The meshes with cells were implanted subcutaneously for 12 weeks. The newly formed bone was evaluated and determined that its formation occurred through EO[22].

Engineered bone strategies through EO process studies combine cells with soft biomaterial scaffolds. However, none of these studies have addressed the potential of using a scaffold system in the load-bearing environment. In this study, we hypothesize that a hybrid scaffold with both a polymer and a gel phase combined together can support bone regeneration via EO in a load-bearing set-up. The gel phase provides the micro-environment to guide the endochondral process, while the polymer phase in the form of a porous graft is expected to provide mechanical strength to the overall polymer-gel structure. Our previous study has showed that a hybrid hydrogel system composed of 70%–30% hyaluronan(HA)-fibrin(FB) is able to mimic stem cell attachment, proliferation, and hypertrophic-cartilage template (HCT) formation[23]. In this study, we propose to combine HA:FB hydrogel with a previously designed optimally porous and biomechanically compatible poly(85% lactide-co-15% glycolide) acid (PLGA 85:15) scaffold to develop a load-bearing polymer-gel hybrid graft[13], [14], [24].

Through this study, a hybrid matrix was developed by combining a gel phase with a load-bearing and porous biodegradable matrix. The hybrid matrix’s ability to support bone

formation through EO was evaluated *in vitro* for hypertrophic-cartilage template formation, and *in vivo* for bone regeneration using a transgenic reporter mouse model.

2. Materials and Methods

2.1. Fabrication of Macro-Porous PLGA Microsphere-Scaffolds

Poly (85% lactide-co-15% glycolide) acid microspheres were prepared using emulsion/solvent evaporation method, as described previously[12]. In brief, PLGA 85/15 (8515 DLG 7E, Evonik Industries, NY, USA) and methylene chloride (L-14119, Fisher Scientific, PA) were mixed in a 1:5 ratio and vortexed until dissolved. The mixture was slowly added to 1% poly vinyl alcohol (Sigma-Aldrich, MO, USA) while stirring at 250 RPM for one hour, after which the stirring continued over night at 300 RPM. The microspheres were then vacuum-dried for 24 hours and sieved. For *in vitro* studies, PLGA 85/15 microspheres (diameter 425–600μm) were combined with porogen (diameter 200–300μm) and prepared as circular matrices of 5mm diameter 2mm thickness. For *in vivo* evaluation, PLGA 85/15 microspheres (diameter 200–300μm) and porogen (diameter 100–200μm) were combined to form 3.5mm diameter × 1mm thickness circular matrices. Both the matrix types were formed with a ratio of 80 PLGA to 20 NaCl, and thermally sintered at 102°C for one hour. The NaCl was then leached out by soaking the composite PLGA/NaCl scaffolds in distilled water for 2 hours, resulting in scaffolds with increased porosity[24]. Washed scaffolds were allowed to air dry and then placed in desiccator for later use.

2.2. Hybrid Matrix Preparation

The PLGA-gel hybrid matrix was prepared by infusing the gel phase into the pore structure of the PLGA polymer matrix[25]. An illustration of the hybrid matrix with cells is shown in Figure 1. Prior to infusion, PLGA scaffolds were sterilized by immersing in 70% ethanol for 15–20 minutes. In aseptic conditions, scaffolds were then washed three times in sterile PBS before exposing them to UV radiation for 10 minutes per side. Scaffolds were then placed in 24-well plates and dried.

The hydrogel phase was prepared by mixing 70% hyaluronan (ESI-BIO Stem Cells Solutions) and 30% fibrin (Sigma Aldrich) in an eppitube. To encapsulate the cells, a predetermined cell suspension volume was resuspended in the hydrogels before the addition of any crosslinker to ensure uniform distribution of cells. PEGSSA (ESI-BIO Stem Cells Solutions) was added first to the gel solution and mixed well, then 50mM $CaCl_2$ and subsequently 20 unit/mL of thrombin (Sigma Aldrich) were added. The hybrid hydrogel was then immediately added to the PLGA scaffold and allowed to crosslink for at least 30 minutes, followed by the addition of phosphate buffered solution or media.

2.3. Human BMSCs Culture

35mL of freshly isolated human bone marrow aspirate (BMA) was purchased from Lonza (Walkersvile, MD). The BMA was processed through *Magellan®* system (Arteriocyts, Hopkinton, MA) to obtain concentrated BMA (cBMA)[26]. Then human bone marrow-derived mesenchymal stem cells (hBMSCs) were obtained by seeding the cBMA onto 150mm culture dishes and cultured at 37°C in humidified atmosphere containing 5% CO_2 in

basal media. Basal media used for the following experiments consisted of Dulbecco's Modified Eagle Medium and Ham's F12 (DMEM/F12, Life Technologies) with Glutamax, 10% fetal bovine serum (FBS, Life Technologies), and 100unit/mL penicillin-streptomycin (P/S, Life Technologies). Culture medium was changed every two days, and cells were passaged when plates reached 70–80% confluency.

2.4. Cell Seeding

Hybrid matrix and PLGA scaffold alone were each seeded with 500,000 hBMSCs and cultured in basal media (as described in Section 2.3) for 21 days at 37°C in humidified atmosphere containing 5% CO_2.

2.5. Live/Dead Assay

Live-dead cell viability assay was performed according to the manufacturer's protocol to label live cells green with Calcein AM, and dead cells red with ethidium homodimer-1 probes after 21 days of culture. Confocal microscopy (Zeiss LSM Meta, 10X magnification) was utilized to image interior cells as well as the surface of the scaffolds.

2.6. PicoGreen Assay

To examine cell proliferation, samples were taken out at 1, 3, 7, 14, and 21 days and evaluated quantitatively using the Quant-iT™ Picogreen dsDNA assay (Invitrogen, USA). The fluorescence of samples and standards were measured for fluorescence at 485nm/535nm using a BioTek plate reader[27].

2.7. Chondrogenic and hypertrophic-chondrogenic priming

To evaluate the matrices' potential to support hypertrophic cartilage template (HCT) formation, hBMSCs seeded on hybrid matrices and polymeric matrices were cultured in chondrogenic media for 14 days followed by 14 days of additional culture in hypertrophic media, as per an established protocol[23]. Chondrogenic media consisted of high glucose DMEM/F12 with Glutamax supplemented with 10nM transforming growth factor-beta 1 (TGF-β_1), Insulin-transferrin-sodium selenite, and linoleic-BSA pre-mix (ITS61), 50mg/mL ascorbate-2-phosphate, 100mg/mL sodium-Pyruvate, 40mg/mL proline and 100nM dexamethasone. The hypertrophic media consisted of high glucose DMEM/F12 with Glutamax with 50nM Thyroxine (T3), 7 mM β-glycerophosphate, ITS+1, 50μg/mL ascorbate-2-phosphate, 100μg/mL sodium-Pyruvate, 40μg/mL proline and 0.01μM dexamethasone. Samples taken out at day 14 and 28 were analyzed for PicoGreen DNA quantification as described in Section 2.6 and for further analysis.

2.8. Dimethylmethylene Blue (DMMB) Assay

Sulfated glycosaminoglycan (sGAGs) production of both chondrogenic and hypertrophic stages were quantitatively measured using DMMB assay as previously described[23]. sGAGs are highly negatively charged molecules and can be measured directly by using a metachromatic dye, 1, 9 Dimethylmethylene blue. The GAG-dye complex results in an absorption spectrum shift which can be measured at 525 nm. Samples were harvested and washed with PBS then digested for 16 hours at 56°C. The digestion buffer consists of Tris/

EDTA buffer, iodoacetamide, pepstatin A, and proteinase K. After digestion, the DMMB solution was added in a 1:1 ratio and the absorbance was immediately measured using a BioTek plate reader at 520 nm wavelength. The measured absorption for each sample was normalized to the amount of DNA (obtained via Picogreen assay).

2.9. Alkaline Phosphatase Activity

Alkaline phosphatase activity (ALP) of both chondrogenic and hypertrophic cultures were measured. ALP is an established marker for chondrogenic hypertrophy. Alkaline phosphatase (ALP) substrate kit (Bio-Rad, Hercules, CA) was used for this purpose. This essay converts p-nitrophenyl phosphate (p-NPP) into p-nitrophenol (p-NP). The rate of p-NP formation is directly proportional to the ALP activity, and it can be measured colorimetrically. addition of 1% After washing with PBS, samples were crushed before the Triton-100X solution. The ALP induced p-NP production was estimated by measuring the absorption using TECAN plate reader at 405 nm wavelength. The results of ALP activity were normalized with the DNA (Picogreen Assay) content of that sample.

2.10. Immunofluorescent Staining for Collagen II and Collagen X

At both the chondrogenic and hypertrophic stages, cells encapsulated in hybrid matrix and PLGA were evaluated for their expression of Col II and Col X. Fluorescence was subsequently visualized using a confocal microscope (LSM 510 Meta, Zeiss, 10X and 20X). A double immunofluorescence-sequential protocol was used. Samples were briefly washed with PBS and blocked with 1% BSA for 30 minutes. Samples were incubated with first a primary antibody, Anti-collagen II (at 1:100 dilution, AB30092) or Anti-collagen X (at 1:400 dilution) in 1% BSA for one hour in a humidified chamber. The primary antibody was removed, and samples were washed with PBS for 5 minutes and repeated three times. Samples were then incubated with first secondary antibody (fluorochrome), Alexa-fluor 546 (1:400 dilution) in PBS for one hour at room temperature. Samples were again washed with PBS for 5 minutes and repeated three times, followed by a second blocking step with 1% BSA for one hour at room temperature. Samples were incubated with a second primary antibody, Anti-collagen II (at 1:100 dilution, AB30092) or Anti-collagen X (at 1:400 dilution) in 1% BSA for one hour in a humidified chamber. The second primary antibody was removed and the samples were washed with PBS for 5 minutes and repeated three times. Samples were then incubated with a second secondary antibody (fluorochrome), Alexa-fluor 488 (1:400 dilution) in PBS for one hour at room temperature. Samples were washed with PBS for 5 minutes and the washing step was repeated three times. Finally, samples were incubated with propidium iodide (1 mg/ml in water or PBS) for 15 minutes at room temperature before imaged under a confocal microscope.

2.11. Endochondral Template Formation and Cellular Attachment

Polymer matrix alone and hybrid matrix were seeded with 500,000 cells and cultured in chondrogenic and hypertrophic media for template formation as described in Sections 2.4 and 2.7. The samples, after template formation, were then transferred into ultra-low attachment plates to further characterize their homing potential in which 50,000

fresh hBMSCs were added with the basal media to the ultra-low attachment plates. The culture was continued for 21 days, after which amount of extracellular calcium deposition was estimated using Alizarin red staining as previously described[24]. Before washing, samples were imaged for representative images of mineralization present in the matrices. This colorimetric analysis is based on solubility of the red matrix precipitate with cetylpyridinium chloride (CPC) to yield a purple solution. Colorimetric changes were measured using a spectrophotometric plate reader at wavelength 562 nm. hBMSCs cultured on tissue culture plates (TCPS) in osteogenic media were used as a control.

2.12. *In Vivo* Calvarial Critical-Size Mouse Model

Hybrid matrix circular discs of 3.5mm diameter × 1mm thickness were prepared as described in Section 2.2. The animal procedures used in this study were approved by the UConn Health Center Institutional Animal Care and Use Committee (IACUC). A total of 12 NOD *scid gamma* (NSG) mice (26–33 g) were bred and raised at UCHC. 500,000 hBMSCs were encapsulated in hybrid matrices or PLGA matrices and cultured in chondrogenic media, containing 10 ng/ml TGF-β_1 for one week. Samples were then implanted into a mouse critical-size calvarial transgenic model NSG/Col3.6tpz. Briefly, the animals (n=6) were anesthetized with a ketamine (135 mg/kg)–xylazine (15 mg/kg) blend and two 3.5-mm-diameter defects were introduced in the right (PLGA) and left (hybrid matrix) parietal lobes using a Dremel MultiPro drill with a trephine bit. After construct placement in the defect, the incision was closed with absorbable VICRYL* (polyglactiin 910) sutures, and the animals were given analgesic (bupronephrine, 0.08mg/kg). Implanted mice were maintained for four and eight weeks. One day before sample harvesting, alizarin complexone (AC) (Sigma-Aldrich, catalog no. 3882) was intraperitoneally injected (30mg/kg in 2% $NaHCO_3$ (pH 7.4)) to label new mineral deposition.

2.13. Histology and X-Ray Imaging

Samples were harvested four and eight weeks post-surgery. Animals were sacrificed by CO_2 asphyxiation, and calvarial samples were harvested, fixed in neutral buffered formalin and imaged by digital x-ray (LX60; Faxitron). Histological samples were prepared using a similar protocol[28], [29]. In brief, each calvarium was soaked overnight in 30%sucrose/PBS solution, covered with an embedding medium (Cryomatrix; Thermo Fisher Scientific and affixed to an aluminum stage for cryosectioning using non-autofluorescent adhesive film (Section LaboratoryCo.,Hiroshima Japan) to capture the sections and transferred to a glass slide using 0.2% chitosan solution dissolved in 0.25% acetic acid. Set of three adjacent sections were collected for histological imaging. For endogenous fluorescence detection and imaging, sections were then rinsed three times in PBS, followed by distilled water, and placed on a glass slide. A 50% glycerol solution was applied to the section, and a glass coverslip was placed on top. This was followed by coverslip removal by PBS for additional staining. Tartrate resistant acid phosphatase (TRAP) enzymatic activity was obtained by soaking the slide in TRAP reaction solution (112mM sodium acetate, 76mM sodium tartrate, 11mM sodium nitrate, pH 4.1–4.3) for 10 mins, followed by addition of ELF 97 substrate (1:20 to 1:60, Life Technologies, E-6588) and exposure to UVB light for 5mins. This was followed by three changes of PBS washing and coverslip mounting for imaging. In addition, alkaline phosphatase (AP) activity staining was done following

previous study[28], [29]. For human nuclear antigen (HuNucAg) antibody staining, adjacent slide sections to TRAP staining were treated with proteinase K, placed in humidified incubator at 37°C for 10 mins, washed in PBS three times, then treated with 0.1% Triton X-100 for 10 mins followed by washing. Slides were then blocked with HuNucAg (MAB1281, Milipore), diluted at 1:200, for 1 hour at RT followed by incubation with donkey anti-mouse Cy3 (Catalog no. 715–166–150, Jackson ImmunoResearch Labs), diluted at 1:500, for 1 hr at RT. Sections were then washed and mounted in 0.1% DAPI in 50% glycerol for imaging. For toluidine blue (TB) staining, sections were washed, stained with 0.025% toluidine blue O (Sigma, Catalog no. T3260), rinsed, placed in bluing solution (Shadon, Cat. No. 6769001), rinsed and mounted in 30% glycerol. Tiled 100x images of the entire calvarial section for each staining step of the same or adjacent section were acquired with the scanning fluorescent microscope (AxioscanZ1; Zeiss) equipped with a digital camera (Axiocan; Zeiss) from which an image stack was created to align the fluorescent signals with the mineralized bone and the TB stain.

2.14. Statistical Analysis

Quantitative data were reported as the mean ± the standard deviation (SD). The comparison between two groups was determined using student's t-test with statistical significance evaluated at $p<0.05$.

3. Results

Hybrid matrices were assembled by infusing a hydrogel phase (70% hyaluronan and 30% fibrin) into a porous PLGA matrix. Prior to infusion, the gel phase was mixed with hBMSCs in order to cellularize the matrices. An illustration of the hybrid matrix is shown in Figure 1. We assessed the matrices for cell survival and proliferation. Live/dead staining shows that hBMSCs in the PLGA group are only present on the microsphere surfaces (Figure 2A). However, in the hybrid matrix cells are localized at the inter-microsphere spaces, where the hydrogel is, as well as the microsphere surfaces. This trend continues through day 21, at which point the hybrid matrix seems fully cellularized. The data shows all groups steadily increase in proliferation from day 1 to day 7 (Figure 2B). At day 14, both the control and the TCPS rapidly decrease in DNA content While in the case of the hybrid matrix, cells continue to proliferate at a steady rate through day 21.

Next, the hybrid matrix was evaluated for its potential to support HCT formation. This included studying cell proliferation during the chondrogenic differentiation, and their further maturation into hypertrophic chondrocytes as presented in Figure 3. Proliferation for the hybrid matrix, at both the chondrogenic and the hypertrophic stages, was significantly higher as shown by the increased DNA content in Figure 3A. To examine the chondrogenic differentiation, sulfated GAGs was quantified using DMMB assay and the results are presented in Figure 3B. The hybrid matrix showed significantly higher sGAG formation at the chondrogenic stage. A slight increase of sGAG expression was observed for the PLGA group at the hypertrophic stage compared to the hybrid matrix. Similarly, the ALP activity was examined as a hypertrophic marker, shown in Figure 3C. Again, the hybrid matrix group showed significantly higher ALP activity at the hypertrophic stage; however, the PLGA

group did show some ALP activity at the chondrogenic stage while no ALP activity was observed in the hybrid matrix at this stage.

Next, key chondrogenic and hypertrophic markers, Col II and Col X, were examined and imaged with a confocal microscope, and the results are presented in Figure 4. At the chondrogenic stage, Col II was expressed only in the hybrid matrix while no evidence of Col X was seen in either group. At the hypertrophic stage, Col X was observed in both the PLGA and the hybrid matrices, with a higher intensity in the hybrid matrix. While Col II was not observed with PLGA, however, a slight expression was still observed in the hybrid matrix at this stage.

After the HCT potential was established, the cellular attachment and osteoinductive potential of the hybrid matrix was indirectly evaluated. Matrices cultured in basal media with fresh hBMSCs were evaluated for subsequent extracellular calcium deposition at day 21. Figure 5 shows the alizarin red staining results of the matrices before (Figure 5A) and after (Figure 5B) the addition of fresh hBMSCs. The PLGA matrix showed only slightly increased calcium deposition after the addition of fresh hBMSCst at a lower intensity than the hBMSCs cultured on TCPS in osteogenic media. The hybrid matrix showed uniform and rich mineral deposition at the template formation stage as shown in Figure 5C. After the addition of fresh hBMSCs, the hybrid matrix samples showed significantly higher calcium deposition and mineralization when cultured in basal media (Figure 5D).

A transgenic reporter-mouse critical-defect calvarial model was used to evaluate the hybrid matrix system *in vivo*. The transgenic reporter mouse (NSG/Col3.6Tpz) contains a Col3.6 promoter driven green fluorescent protein (GFP) used for ease of tracking and distinguishing host (mouse) cells versus implanted hBMSCs. In this study, one-week-old pre-chondrogenic samples were implanted on the right (PLGA matrix) and left (hybrid matrix) side of the parietal lobe in a 3.5 mm size calvarial defect and analyzed after four and eight weeks (n=6). Individual samples were monitored by digital images, X-ray, and histology. The digital images, Figure 6A and C, show that the hybrid matrix samples are in place with no shifting or dislocation four and eight weeks post-implantation. The same can be said for the PLGA scaffold at four weeks, however, in this particular representative image that was used, there was shifting at eight weeks post-implantation. The images also indicate healthy tissue surrounding the samples, with no appearance of inflammation or scar tissue formation. Figure 6B and D show the mineralization of each sample using X-ray imaging at weeks four and eight. At week four, mineralization is more evident in the hybrid matrix, with little to no mineralization in the PLGA matrix. After eight weeks, the hybrid matrix showed significantly more areas of mineralization with higher mineral density/intensity compared to four week, especially around the defect perimeter. At both week four and eight, these areas of mineralization are scattered throughout the samples, however, increased bone intensity was observed at the later time point.

The samples were also sectioned and stained to study the distribution and contribution of both hBMSCs and mouse calvarial cells in the bone regeneration process. Histological imaging at four weeks post-implantation is displayed in Figure 7. The overall composition of both the hybrid and PLGA matrix at four weeks is displayed (Figure 7A) by merging TB,

GFP signal and accumulated mineral formation. At four weeks, some mineralization and bone formation was observed within the defect site of the hybrid matrix group (Figure 7A). It was clear that there was no mineralization present at week four within the PLGA matrix group, therefore, the rest of the histological imaging analysis was focused solely on the hybrid matrices in order to analyze the bone formation. Two different magnified regions were selected from these images for subsequent analysis, region 1 (B,C,D,E) and region 2 (F). TB staining was kept throughout all of the images (Figure 7A–F) in order to give a consistent background and for perspective purposes of cellular and mineral context.

At four weeks, the green fluorescence protein (GFP) signal from the NSG/Col3.6Tpz mice is clearly seen. These GFP-positive cells are co-localized on the surfaces of mineralization edges (Figure 7B). For Figure 7C, AC was injected 24 hours prior to sacrifice to allow for identification of newly formed bone mineralization within that time period. By overlaying AC and GFP signal, it was revealed that newly formed mineralization is observed to be co-localized with the GFP signal. Likewise, the AP signal, an indicator of an active osteoblast, was revealed to be expressed surrounding these regions of new mineralization and GFP signal presence. Furthermore, TRAP staining was used to identify osteoclast activity to evaluate the remodeling potential of newly formed bone and was observed to be slightly expressed within these areas of new bone formation and GFP presence. Lastly in region 2, the presence of both seeded hBMSCs by human nuclear antigen (HuNuc Ag) signal as well as host cells by GFP signal was observed within the hybrid matrices (Figure 7E).

Histological sections eight weeks post-implantation are presented in Figure 8. These observations were similar to what was seen at week four with increased areas of high-density mineralization. This mineralization is co-localized with GFP-positive cells on the surfaces (Figure 8B). The trend of AC staining and AP activity continued at week eight, Figure 8C and 8D, surrounding the surfaces of the mineralization Similarly, an increase in the presence of TRAP staining was observed within these same areas of new mineralization at eight weeks, Additionally, HuNucAg in Figure 8F revealed the increased presence of hBMSCs (donor cells) on the hybrid matrix surrounded by GFP signal (host cells). Overall, the histological staining at week eight showed higher density mineralization, AP-positive cells and remodeling of newly formed bone compared to week four.

4. Discussion

Biodegradable hydrogels alone or with some form of calcium phosphate have been studied for cartilage mediated bone regeneration[17], [30]–[32]. In order to apply this method for large or segmental bone defect repair, development of weight-bearing scaffolds that promote bone regeneration via EO is warranted. Through this work, the development of a mechanically stable hybrid polymeric-gel matrix for bone defect repair via EO was assessed.

We previously developed and investigated a series of hyaluronic acid – fibrin gel combinations for its ability to serve as a transitionary ECM for hBMSCs to proliferate and establish a healthy HCT [23]. These studies identified 70 HA-30 FB gel as an optimal composition to support chondrogenic and subsequent hypertrophic behavior with superior cell micro-aggregation and differentiation[23]. PLGA 85/15 matrix was chosen as a load-

bearing structure for hybrid scaffold fabrication. We chose PLGA 85/15 as an example template, however, any biodegradable matrix with weight-bearing properties can be utilized to develop hybrid matrices. While the hydrogel composition did not change for all *in vitro* and *in vivo* studies, the size of PLGA microspheres and porogen were different. Similar to previous work in our group; all *in vitro* studies were performed using PLGA microspheres in the range of 425–600μm and NaCl in the 200–300μm diameter range[13], [14], [24]. However, to design matrices with dimensions suitable for a critical-size defect mouse model, PLGA microspheres of 200–300μm in diameter and NaCl of 100–200μm in diameter were combined and thermally sintered to form 3.5mm diameter × 1mm thickness circular matrices. The scaffold composition and conditions were chosen based on the previous studies to produce scaffolds that display mechanical properties in the range of human cancellous bone while supporting cell survival and growth throughout the structure[13], [14], [24].

The hybrid matrix with hBMSCs was assessed for cell proliferation, HCT formation, and subsequent ossification. Cell proliferation for the hybrid matrix continued to increase up to day 21, while both PLGA and TCPS groups show somewhat decreased DNA content at day 14 and 21. This may be because of the fact that the PLGA porous matrix provides limited surface area for cell growth. Conversely, the hybrid matrix offers additional surface through the hydrogel phase. The live/dead images support these findings (Figure 2A), where cells in the polymeric microsphere matrix without the gel phase are limited to the microsphere surfaces whereas the hybrid matrices show cells both on the microsphere surfaces as well in the void-area, within the hydrogel phase.

The matrices' HCT formation potential was examined for both matrix groups. GAGs are a major component for the chondrogenic extracellular matrix whereas ALP is an established marker for chondrogenic hypertrophy therefore; DMMB assay and ALP was used to quantitatively assess sGAG expression and ALP activity. Both sGAG formation and ALP activity were significantly higher in hybrid matrix in their prospective stages, Figure 3B and C. Interestingly, the PLGA matrix exhibited increased sGAG formation at the hypertrophic stages, supporting the notion that differentiation of hBMSCs was delayed in this group. While the decreased sGAG presence in the hybrid matrix during the hypertrophic stage indicates the presence of the transient cartilage phase that occurred in the chondrogenic media and its reduction during the hypertrophic stage. This is possibly due to the breakdown of GAG that helps form the mineralization process as demonstrated by the increased ALP activity/bone formation activity at this phase[33]. No ALP activity was observed for the hybrid matrix at the chondrogenic stage further supporting the indication of a healthy transition of hMSCs into chondrocytes without early mineralization. To further verify the stage at which the hBMSCs within the matrices are in, key chondrogenic and hypertrophic markers, Col II and Col X, were examined. The increased Col II presence in the hybrid matrix at the chondrogenic phase and Col X at the hypertrophic phase provides additional evidence of the healthy transition of the hBMSCs when cultured on these matrices. These findings were similar to a study performed by Mueller et al., where MSC pellet cultures primed in chondrogenic media for 2 weeks followed by hypertrophy inducement led to increased ALP activity and Col X expression[34].

The ultimate goal of this study was to establish the osteogenic potential of the engineered hybrid matrix through EO. Therefore, the “homing” potential, or the matrix’s ability to recruit host cells for the continuation of EO after the hypertrophic stage, was also evaluated by suspending fresh hBMSCs in basal media along with hybrid matrix after a HCT was formed. Consequently, the new hBMSCs are made available for recruitment by and attachment to the matrices. When fresh hBMSCs were added hybrid matrix samples showed significantly higher calcium deposition, even in the absence of differentiation media, indicating the osteoinduction potential of the hybrid matrices. From these combined results, it is proposed that the formation of a rich and uniform endochondral template will lead to uniform cell homing and thus the potential subsequent osteogenesis and vascularization that most BTE strategies currently lack.

The enhanced mineralization *in vitro* is due to the hybrid matrix’s ability to support the formation of a rich HCT and may be because of two reasons. (i) The cells that are currently in the hypertrophic phase may be directly causing the calcium deposition and ossification that is present or, (ii) these cells instead may be producing factors that recruit the freshly seeded hBMSCs and cause their subsequent osteogenic differentiation, leading to the increased mineralization that is observed (Figure 5D). This hypothesis is supported given that hypertrophic chondrocytes during their maturation secrete factors that are capable of promoting cell infiltration and ossification such as BMPs, VEGFs, TGF-βs and MMPs[35]–[37]. As the template degrades over time and growth factors are released, fresh hBMSCs are recruited and differentiated into new bone-forming cells[22], [38]. In this study, fresh hBMSCs were added to the established HCT with basal media, no growth factors or chemical agents were added. The *in vitro* mineralization studies revealed that the matrices beyond the hypertrophic cartilage phase were capable of recruiting freshly seeded hBMSCs and induce them towards osteogenic lineage (even in the presence of non-osteogenic media).

In vivo studies to investigate bone formation via endochondral ossification utilized subcutaneous, cranium and segmental defect models. [17], [22], [39]–[43]. The long bone defect model is the appropriate model to use to study EO bone formation since this process naturally forms long bones. However, well-established cranium models with cell tracking ability have the capability to provide valuable information such as how the donor/host cells participate in the bone formation process. For that reason, we chose a cranium model for this pilot study; however, further studies will test these matrices in a load-bearing defect model to study bone formation via EO. Additionally, previous studies have established the biocompatible nature of the materials used in this study (PLGA, hyaluronic acid and fibrin) [13], [21], [44], [45]. Therefore a well-characterized immunocompromised transgenic reporter-mouse (NSG/Col3.6Tpz) critical-calvarial defect model was chosen due to the tracking ability of the model to distinguish host cells from the donor hBMSCs and establish host/donor cell contribution[26], [46], [47]. Previous studies using this model observed complete defect closure at week 4 with more mature, lamellar bone that is similar to native bone at 8 weeks post-implantation[42], [47]. Therefore, the studies here adopted 4 and 8-week time points for analysis. The qualitative assessments of the results suggest that the hybrid matrix was capable of supporting mineral deposition and bone regeneration *in vivo*. The X-ray images showed higher mineral deposition at four weeks for hybrid matrix, which further increased by week eight (Figure 6B and D). X-ray images provide a good qualitative

representation of mineral deposition over time, but they do not indicate the origin of mineralization. Therefore, histological sections were stained to map the contribution of host and donor cells to the repair process and to address the hybrid matrix's ability to induce HCT *in vivo* and promote bone formation.

Active bone formation was assessed by cell presence, mineral deposition and osteoclast activity. By superimposing two or more histological images, we were able to map the various histological staining to the defect sites and determine the origin of new bone formation. At both time points, the hybrid matrices had an increased GFP signal, indicating that these hybrid matrices are effective at attracting host cells through chemotaxis. The increased AC associated with the host cells within the hybrid matrices further supports the origin of new bone formation that occurs. Similarly, the increased AP activity provides evidence that these host cells are in fact AP-positive bone cells, indicating the hybrid matrices ability to not only recruit host cells, but also release factors that aid in bone formation. Therefore, the enhanced bone formation associated with the hybrid matrices could be attributed to the fact that these grafts have the ability to attract stem cells the way they did *in vitro* (when cultured with fresh hBMSCs) and induce bone formation. These results are in corroboration with the study by Farrell et al. in which MSCs were cultured in chondrogenic media followed by subcutaneous implantation into an immunocompetent transgenic rat model[48]. They observed increased bone formation in samples primed in chondrogenic media compared to samples cultured in osteogenic media, similar to our study[48].

In addition, the TRAP staining adjacent to the new mineralization indicated presence of osteoclasts, which is evident of remodeling activity of the newly formed bone at week four and its continued and increased expression at week eight points towards the continued remodeling activity by these cells in the hybrid matrix. The presence of donor cells is noticeably absent surrounding the mineralization within these areas of new bone formation, however, the donor-host cell proximity observed (Figures 7F and 8F) suggest that the donor cells may be responsible for recruiting host cells and their contribution to mineralization observed at both week four and eight. This claim is supported by previous studies in which implanted cell-laden hydrogel systems demonstrated *in vivo* bone formation by the encapsulated donor MSCs[49]–[51].

Previous literature has shown that the length of "priming" or pre-conditioning of cells prior to implantation has an influence on bone regeneration, showing that longer preconditioning of hBMSCs prior to implantation leads to better EO *in vivo* [26], [38], [52]. Conversely, studies by Yang et al. reported implanted constructs following 2, 3 and 4 weeks of priming in chondrogenic media gave rise to EO bone formation in which the bone volume was not affected by length of priming time[53]. In addition, Knuth et al. demonstrated MSC-mediated bone formation following just 7 day of *in vitro* priming[54]. In the present case, we limited our investigation to one week of priming prior to implantation, to observe whether it would be sufficient enough to induce bone formation. Further studies in a long-bone defect model will look at a range of in vitro priming (1–4 weeks) in order to establish the minimum length of priming that is required to induce bone formation via EO. In addition, the chosen model was a flat bone model in which the bone regeneration mostly

occurs via IO; a suitable long bone defect model is needed for proper *in vivo* assessment of whether these scaffolds are capable of promoting bone regeneration via EO. We believe that these two factors played a significant role in our study that favored bone regeneration via IO *in vivo*. However, the *in vitro* studies done here, and previously[23], have suggested that the matrix has the capability to provide the right conditions to support bone regeneration via EO as well as has showed much better results in terms of bone formation at weeks four and eight.

The host cell recruitment by the hybrid matrix and their co-localization with the subsequent bone mineralization and remodeling suggests that these polymeric-hydrogel hybrid scaffolds are capable of supporting mineral deposition and bone formation *in vivo*. The use of transgenic mice was particularly helpful as it provided the ability to distinguish between host and donor cells as typical histological analysis is not capable of making such a distinction. Through this it was found that the matrices were able to support donor cells well into eight weeks post-implantation. In addition, these cells seemed to be surrounding/interacting with host cells, possibly aiding in the bone formation that is present.

5. Conclusion

In conclusion, we designed and developed a hybrid matrix and evaluated its ability to support cartilage mediated bone regeneration. The hybrid matrix seeded with human MSCs allowed hypertrophic cartilage template formation when primed *in vitro*. Cellular attachment and mineralization studies indicated the potential of the hybrid matrix to attract stem cells and cause osteogenic differentiation. *In vivo* mineralization/new bone formation in a transgenic mouse calvarial defect model demonstrated the newly developed matrix's ability to recruit host cells and regenerate bone. *In vivo* data further confirmed the newly formed mineral is co-localized with host cells and more over it is actively remodeled. Together, the study developed a hybrid and load-bearing matrix for bone regeneration via endochondral ossification.

ACKNOWLEDGEMENT

The authors acknowledge funding from NSF EFRI (#1332329) and NSF EFMA (#1640008). Dr. Nukavarapu also acknowledges support from the National Institute of Biomedical Imaging and Bioengineering of the National Institutes of Health (#R01EB020640).

References:

[1]. Jahangir A, Nunley R, Mehta S, and Sharan A, "Bone-graft substitutes in orthopaedic surgery," AAOS January Ed, vol. 2, 2008.

[2]. Francois E, Dorcemus D, and Nukavarapu S, "1 - Biomaterials and scaffolds for musculoskeletal tissue engineering," in Regenerative Engineering of Musculoskeletal Tissues and Interfaces, Nukavarapu SP, Freeman JW, and Laurencin CT, Eds. Woodhead Publishing, 2015, pp. 3–23.

[3]. Amini AR, Laurencin CT, and Nukavarapu SP, "Bone Tissue Engineering: Recent Advances and Challenges," Crit. Rev. Biomed. Eng, vol. 40, no. 5, pp. 363–408, 2012. [PubMed: 23339648]

[4]. Roddy E, DeBaun MR, Daoud-Gray A, Yang YP, and Gardner MJ, "Treatment of critical-sized bone defects: clinical and tissue engineering perspectives," Eur. J. Orthop. Surg. Traumatol, vol. 28, no. 3, pp. 351–362, 4 2018. [PubMed: 29080923]

[5]. Goldberg VM and Stevenson S, “Natural history of autografts and allografts,” Clin. Orthop, no. 225, pp. 7–16, 12 1987.

[6]. Vining NC, Warme WJ, and Mosca VS, “Comparison of Structural Bone Autografts and Allografts in Pediatric Foot Surgery:,” J. Pediatr. Orthop, vol. 32, no. 7, pp. 714–718, 2012.

[7]. Karande T and Agrawal C, “Function and Requirement of Synthetic Scaffolds in Tissue Engineering,” CRC Press Boca Raton, 2008.

[8]. Khan Y, Yaszemski MJ, Mikos AG, and Laurencin CT, “Tissue Engineering of Bone: Material and Matrix Considerations,” J. Bone Jt. Surg.-Am. Vol, vol. 90, pp. 36–42, 2 2008.

[9]. Vallet-Regí M and González-Calbet JM, “Calcium phosphates as substitution of bone tissues,” Prog. Solid State Chem, vol. 32, no. 1, pp. 1–31, 1 2004.

[10]. Zhou H and Lee J, “Nanoscale hydroxyapatite particles for bone tissue engineering,” Acta Biomater, vol. 7, no. 7, pp. 2769–2781, 7 2011. [PubMed: 21440094]

[11]. Swetha M, Sahithi K, Moorthi A, Srinivasan N, Ramasamy K, and Selvamurugan N, “Biocomposites containing natural polymers and hydroxyapatite for bone tissue engineering,” Int. J. Biol. Macromol, vol. 47, no. 1, pp. 1–4, 7 2010. [PubMed: 20361991]

[12]. Nukavarapu SP et al., “Polyphosphazene/Nano-Hydroxyapatite Composite Microsphere Scaffolds for Bone Tissue Engineering,” Biomacromolecules, vol. 9, no. 7, pp. 1818–1825, 7 2008. [PubMed: 18517248]

[13]. Amini AR and Nukavarapu SP, “Oxygen-Tension Controlled Matrices for Enhanced Osteogenic Cell Survival and Performance,” Ann. Biomed. Eng, vol. 42, no. 6, pp. 1261–1270, 6 2014. [PubMed: 24570389]

[14]. Amini AR, Xu TO, Chidambaram RM, and Nukavarapu SP, “Oxygen Tension-Controlled Matrices with Osteogenic and Vasculogenic Cells for Vascularized Bone Regeneration In Vivo,” Tissue Eng. Part A, vol. 22, no. 7–8, pp. 610–620, 2 2016. [PubMed: 26914219]

[15]. Mikael PE et al., “Functionalized carbon nanotube reinforced scaffolds for bone regenerative engineering: fabrication, in vitro and in vivo evaluation,” Biomed. Mater, vol. 9, no. 3, p. 035001, 3 2014. [PubMed: 24687391]

[16]. Almubarak S et al., “Tissue Engineering Strategies for Promoting Vascularized Bone Regeneration,” Bone, vol. 83, pp. 197–209, 2 2016. [PubMed: 26608518]

[17]. Sheehy EJ, Vinardell T, Buckley CT, and Kelly DJ, “Engineering osteochondral constructs through spatial regulation of endochondral ossification,” Acta Biomater, vol. 9, no. 3, pp. 5484–5492, 3 2013. [PubMed: 23159563]

[18]. Dennis SC, Berkland CJ, Bonewald LF, and Detamore MS, “Endochondral Ossification for Enhancing Bone Regeneration: Converging Native Extracellular Matrix Biomaterials and Developmental Engineering In Vivo,” Tissue Eng. Part B Rev, vol. 21, no. 3, pp. 247–266, 6 2015. [PubMed: 25336144]

[19]. Thompson EM, Matsiko A, Farrell E, Kelly DJ, and O’Brien FJ, “Recapitulating endochondral ossification: a promising route to in vivo bone regeneration,” J. Tissue Eng. Regen. Med, vol. 9, no. 8, pp. 889–902, 2015. [PubMed: 24916192]

[20]. Zhou Y, Chen F, Ho ST, Woodruff MA, Lim TM, and Hutmacher DW, “Combined marrow stromal cell-sheet techniques and high-strength biodegradable composite scaffolds for engineered functional bone grafts,” Biomaterials, vol. 28, no. 5, pp. 814–824, 2 2007. [PubMed: 17045643]

[21]. Harada N et al., “Bone regeneration in a massive rat femur defect through endochondral ossification achieved with chondrogenically differentiated MSCs in a degradable scaffold,” Biomaterials, vol. 35, no. 27, pp. 7800–7810, 9 2014. [PubMed: 24952976]

[22]. Scotti C et al., “Engineering of a functional bone organ through endochondral ossification,” Proc. Natl. Acad. Sci. U. S. A, vol. 110, no. 10, pp. 3997–4002, 3 2013. [PubMed: 23401508]

[23]. Mikael PE, Kim HS, and Nukavarapu SP, “Hybrid extracellular matrix design for cartilage-mediated bone regeneration,” J. Biomed. Mater. Res. B Appl. Biomater, vol. 106, no. 1, pp. 300–309, 2018. [PubMed: 28140522]

[24]. Amini AR, Adams DJ, Laurencin CT, and Nukavarapu SP, “Optimally Porous and Biomechanically Compatible Scaffolds for Large-Area Bone Regeneration,” Tissue Eng. Part A, vol. 18, no. 13–14, pp. 1376–1388, 7 2012. [PubMed: 22401817]

[25]. Igwe JC, Mikael PE, and Nukavarapu SP, “Design, fabrication and in vitro evaluation of a novel polymer-hydrogel hybrid scaffold for bone tissue engineering,” J. Tissue Eng. Regen. Med, vol. 8, no. 2, pp. 131–142, 2014. [PubMed: 22689304]

[26]. Mikael PE et al., “A potential translational approach for bone tissue engineering through endochondral ossification,” in 2014 36th Annual International Conference of the IEEE Engineering in Medicine and Biology Society, 2014, pp. 3925–3928.

[27]. Xu TO, Kim HS, Stahl T, and Nukavarapu SP, “Self-neutralizing PLGA/magnesium composites as novel biomaterials for tissue engineering,” Biomed. Mater, vol. 13, no. 3, p. 035013, 3 2018. [PubMed: 29362293]

[28]. Xin X et al., “A Site-Specific Integrated Col2.3GFP Reporter Identifies Osteoblasts Within Mineralized Tissue Formed In Vivo by Human Embryonic Stem Cells,” Stem Cells Transl. Med, vol. 3, no. 10, pp. 1125–1137, 10 2014. [PubMed: 25122686]

[29]. Xin X et al., “Histological criteria that distinguish human and mouse bone formed within a mouse skeletal repair defect,” J. Histochem. Cytochem, In press.

[30]. Douglas TEL et al., “Enzymatic mineralization of gellan gum hydrogel for bone tissue-engineering applications and its enhancement by polydopamine,” J. Tissue Eng. Regen. Med, vol. 8, no. 11, pp. 906–918, 2014. [PubMed: 23038649]

[31]. Sheehy EJ, Mesallati T, Kelly L, Vinardell T, Buckley CT, and Kelly DJ, “Tissue Engineering Whole Bones Through Endochondral Ossification: Regenerating the Distal Phalanx,” BioResearch Open Access, vol. 4, no. 1, pp. 229–241, 4 2015. [PubMed: 26309799]

[32]. Sathi GA et al., “Early Initiation of Endochondral Ossification of Mouse Femur Cultured in Hydrogel with Different Mechanical Stiffness,” Tissue Eng. Part C Methods, vol. 21, no. 6, pp. 567–575, 6 2015. [PubMed: 25381834]

[33]. Gabay O et al., “Sirt1-deficient mice exhibit an altered cartilage phenotype,” Jt. Bone Spine Rev. Rhum, vol. 80, no. 6, pp. 613–620, 12 2013.

[34]. Mueller MB and Tuan RS, “Functional Characterization of Hypertrophy in Chondrogenesis of Human Mesenchymal Stem Cells,” Arthritis Rheum, vol. 58, no. 5, pp. 1377–1388, 5 2008. [PubMed: 18438858]

[35]. Deckers MML, Karperien M, van der Bent C, Yamashita T, Papapoulos SE, and Löwik CWGM, “Expression of Vascular Endothelial Growth Factors and Their Receptors during Osteoblast Differentiation,” Endocrinology, vol. 141, no. 5, pp. 1667–1674, 5 2000. [PubMed: 10803575]

[36]. Aghajanian P and Mohan S, “The art of building bone: emerging role of chondrocyte-to-osteoblast transdifferentiation in endochondral ossification,” Bone Res, vol. 6, 6 2018.

[37]. Behonick DJ et al., “Role of Matrix Metalloproteinase 13 in Both Endochondral and Intramembranous Ossification during Skeletal Regeneration,” PLoS ONE, vol. 2, no. 11, 11 2007.

[38]. Scotti C et al., “Recapitulation of endochondral bone formation using human adult mesenchymal stem cells as a paradigm for developmental engineering,” Proc. Natl. Acad. Sci. U. S. A, vol. 107, no. 16, pp. 7251–7256, 4 2010. [PubMed: 20406908]

[39]. Yang W, Yang F, Wang Y, Both SK, and Jansen JA, “In vivo bone generation via the endochondral pathway on three-dimensional electrospun fibers,” Acta Biomater, vol. 9, no. 1, pp. 4505–4512, 1 2013. [PubMed: 23059416]

[40]. Bahney CS et al., “Stem Cell–Derived Endochondral Cartilage Stimulates Bone Healing by Tissue Transformation,” J. Bone Miner. Res, vol. 29, no. 5, pp. 1269–1282, 2014. [PubMed: 24259230]

[41]. Lin D, Chai Y, Ma Y, Duan B, Yuan Y, and Liu C, “Rapid initiation of guided bone regeneration driven by spatiotemporal delivery of IL-8 and BMP-2 from hierarchical MBG-based scaffold,” Biomaterials, vol. 196, pp. 122–137, 3 2019. [PubMed: 29449015]

[42]. V Gohil S, Brittain SB, Kan H-M, Drissi H, Rowe DW, and Nair LS, “Evaluation of enzymatically crosslinked injectable glycol chitosan hydrogel,” J. Mater. Chem. B, vol. 3, no. 27, pp. 5511–5522, 2015. [PubMed: 32262522]

[43]. Gohil SV, Wang L, Rowe DW, and Nair LS, “Spatially controlled rhBMP-2 mediated calvarial bone formation in a transgenic mouse model,” Int. J. Biol. Macromol, vol. 106, pp. 1159–1165, 1 2018. [PubMed: 28847606]

[44]. Anderson JM and Shive MS, “Biodegradation and biocompatibility of PLA and PLGA microspheres,” Adv. Drug Deliv. Rev, vol. 28, no. 1, pp. 5–24, 10 1997. [PubMed: 10837562]

[45]. Snyder TN, Madhavan K, Intrator M, Dregalla RC, and Park D, “A fibrin/hyaluronic acid hydrogel for the delivery of mesenchymal stem cells and potential for articular cartilage repair,” J. Biol. Eng, vol. 8, p. 10, 5 2014. [PubMed: 25061479]

[46]. Villa MM, Wang L, Huang J, Rowe DW, and Wei M, “Visualizing Osteogenesis In Vivo Within a Cell–Scaffold Construct for Bone Tissue Engineering Using Two-Photon Microscopy,” Tissue Eng. Part C Methods, vol. 19, no. 11, pp. 839–849, 11 2013. [PubMed: 23641794]

[47]. Gohil SV, Adams DJ, Maye P, Rowe DW, and Nair LS, “Evaluation of rhBMP-2 and bone marrow derived stromal cell mediated bone regeneration using transgenic fluorescent protein reporter mice,” J. Biomed. Mater. Res. A, vol. 102, no. 12, pp. 4568–4580, 2014. [PubMed: 24677665]

[48]. Farrell E et al., “In-vivo generation of bone via endochondral ossification by in-vitro chondrogenic priming of adult human and rat mesenchymal stem cells,” BMC Musculoskelet. Disord, vol. 12, no. 1, p. 31, 1 2011. [PubMed: 21281488]

[49]. Zhao X et al., “Injectable Stem Cell-Laden Photocrosslinkable Microspheres Fabricated Using Microfluidics for Rapid Generation of Osteogenic Tissue Constructs,” Adv. Funct. Mater, vol. 26, no. 17, pp. 2809–2819, 2016.

[50]. Visser J et al., “Endochondral bone formation in gelatin methacrylamide hydrogel with embedded cartilage-derived matrix particles,” Biomaterials, vol. 37, pp. 174–182, 1 2015. [PubMed: 25453948]

[51]. Vo TN et al., “Injectable Dual-Gelling Cell-Laden Composite Hydrogels for Bone Tissue Engineering,” Biomaterials, vol. 83, pp. 1–11, 3 2016. [PubMed: 26773659]

[52]. Freeman FE, Haugh MG, and McNamara LM, “Investigation of the optimal timing for chondrogenic priming of MSCs to enhance osteogenic differentiation in vitro as a bone tissue engineering strategy,” J. Tissue Eng. Regen. Med, vol. 10, no. 4, pp. E250–E262, 2016. [PubMed: 23922276]

[53]. Yang W, Both SK, van Osch GJVM, Wang Y, Jansen JA, and Yang F, “Effects of in vitro chondrogenic priming time of bone-marrow-derived mesenchymal stromal cells on in vivo endochondral bone formation,” Acta Biomater, vol. 13, pp. 254–265, 2 2015. [PubMed: 25463490]

[54]. Knuth C, Witte-Bouma J, Ridwan Y, Wolvius E, and Farrell E, “Mesnchymal Stem Cell-Mediated Enchodondral Ossification Utilising Micropellets and Brief Chondrogenic Priming,” Eur. Cell. Mater, vol. 34, pp. 142–161, 2017. [PubMed: 28937176]

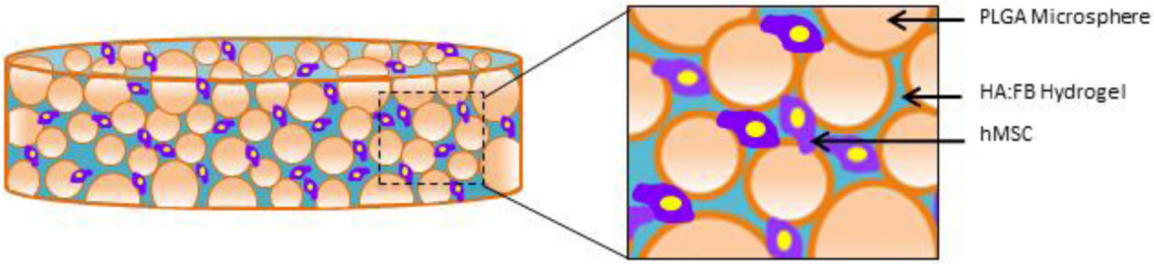

Figure 1.

Hybrid matrix scaffold design: Illustration of the hybrid polymer-gel matrix. The PLGA polymer matrix provides mechanical stability, while the (hyaluronic acid-fibrin) gel-phase is expected to support the seeded MSC chondrogenesis, hypertrophy and bone formation. Overall, the matrix is designed to support bone regeneration via endochondral ossification in a load-bearing structure.

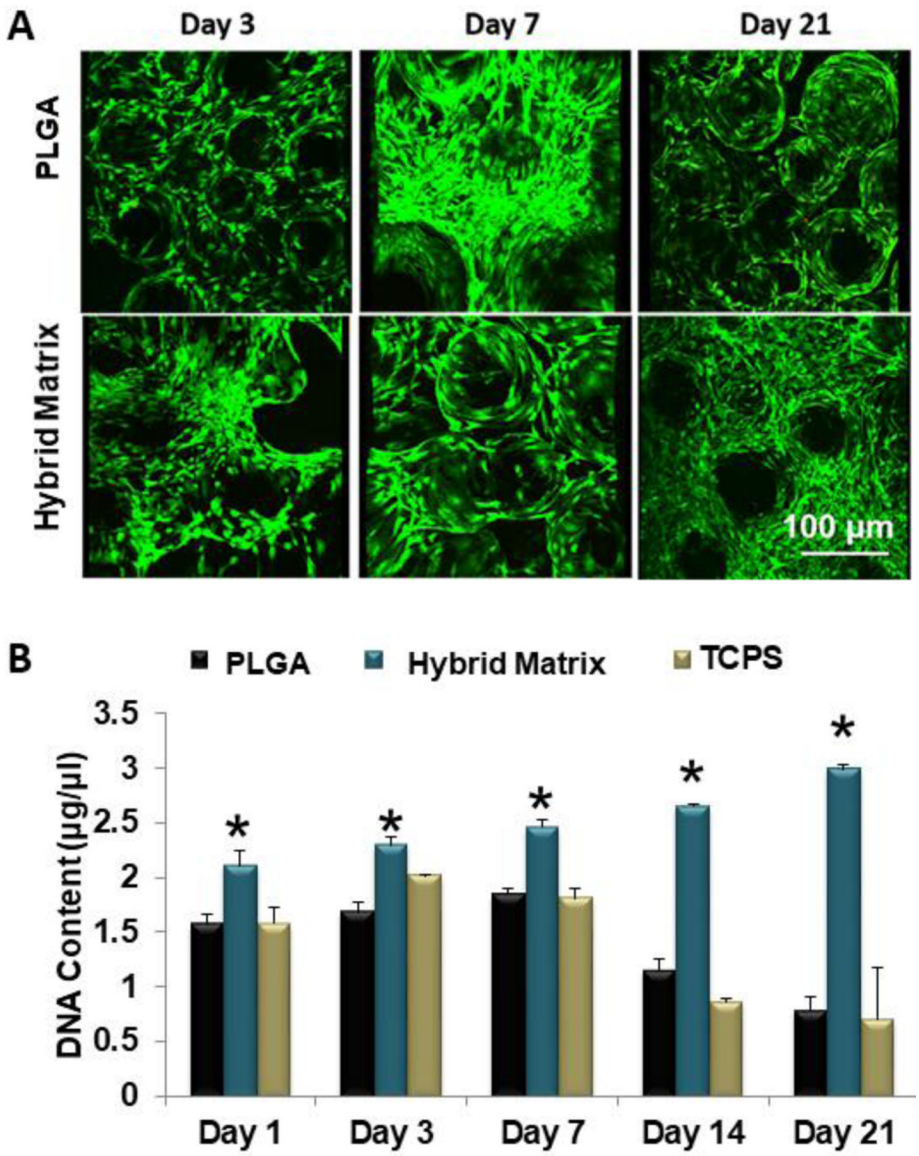

Figure 2.

MSC survival and growth: (A) Growth and survival of hBMSCs cells in hybrid matrix and PLGA alone scaffold. Images show live and dead cells cultured in hybrid matrix: green represents live cells and red represents dead cells. Images were recorded at 10x magnification. (B) hBMSC proliferation in PLGA matrix, hybrid matrix and TCPS. Results of Picogreen assay showing DNA content of hBMSCs cultured in PLGA matrix, hybrid matrix and TCPS for 1, 3, 7, 14 and 21 days. Hybrid matrix shows significantly higher DNA content for all time points through day 21, while PLGA matrix and TCPS decline after day 7 (n=3, $p<0.05$).

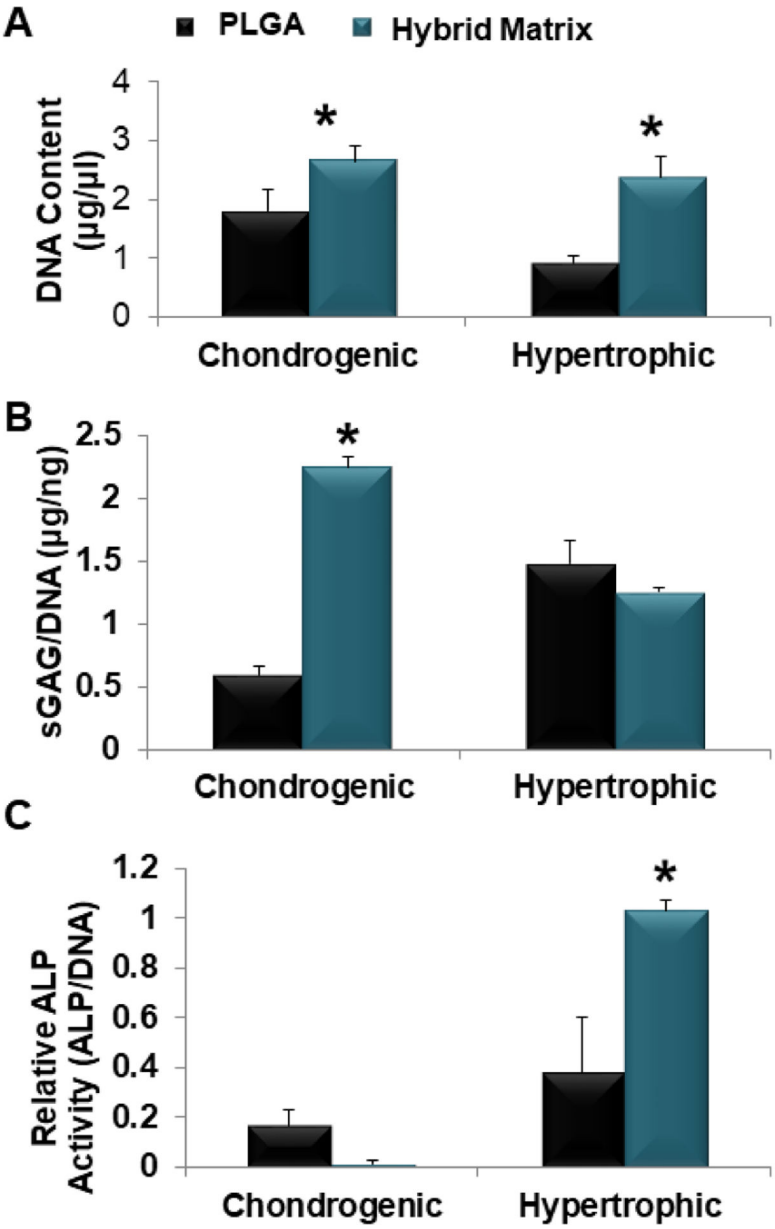

Figure 3.

MSC chondrogenesis and hypertrophy. hBMSCs seeded within PLGA and hybrid matrix and cultured in chondrogenic media for two weeks for analysis or followed by an additional two week culture in hypertrophic media (A) hBMSCs proliferation in PLGA and hybrid matrix during the hypertrophic-cartilage template formation. Results of Picogreen assay showing DNA content of hBMSCs cultured in hybrid matrix was significantly higher than PLGA at both time points. (B) Quantitative analysis of sGAG formation. Dimethyl methylene blue (DMMB) assay was used to quantify glycosaminoglycan production and results are normalized to DNA content (Picogreen) (n=3, $p<0.05$). (C) Quantitative analysis of ALP activity. ALP activity levels and results are normalized to DNA content (Picogreen). (n=3, $p<0.05$).

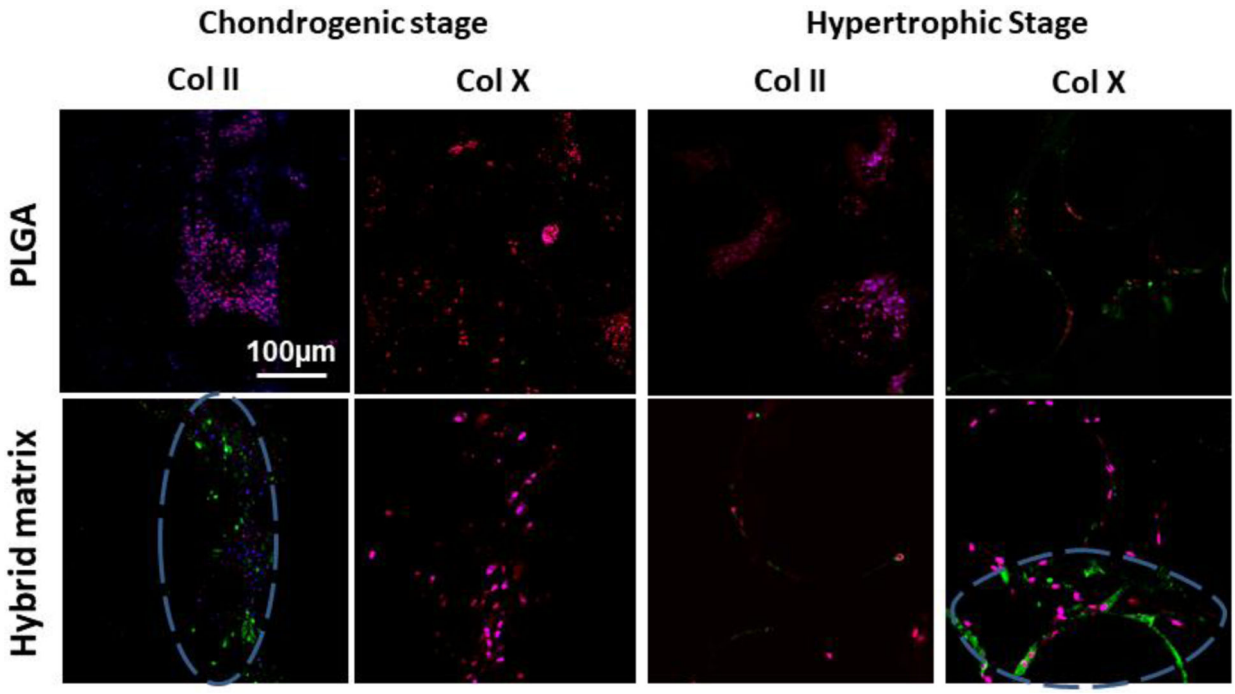

Figure 4.

Chondrogenic and Hypertrophic template confirmation via Collagen II and Collagen X expression: Confocal microscopy images of Collagen II and Collagen X expression in chondrogenic and hypertrophic chondrocytes, respectively. Col II and X expressions were stained green, nucleus in blue, and tubulin in red (10X magnification). Blue dashed circle represents regions of interest demonstrating Col II and Col X that was expressed in the hybrid matrix in their respective stages.

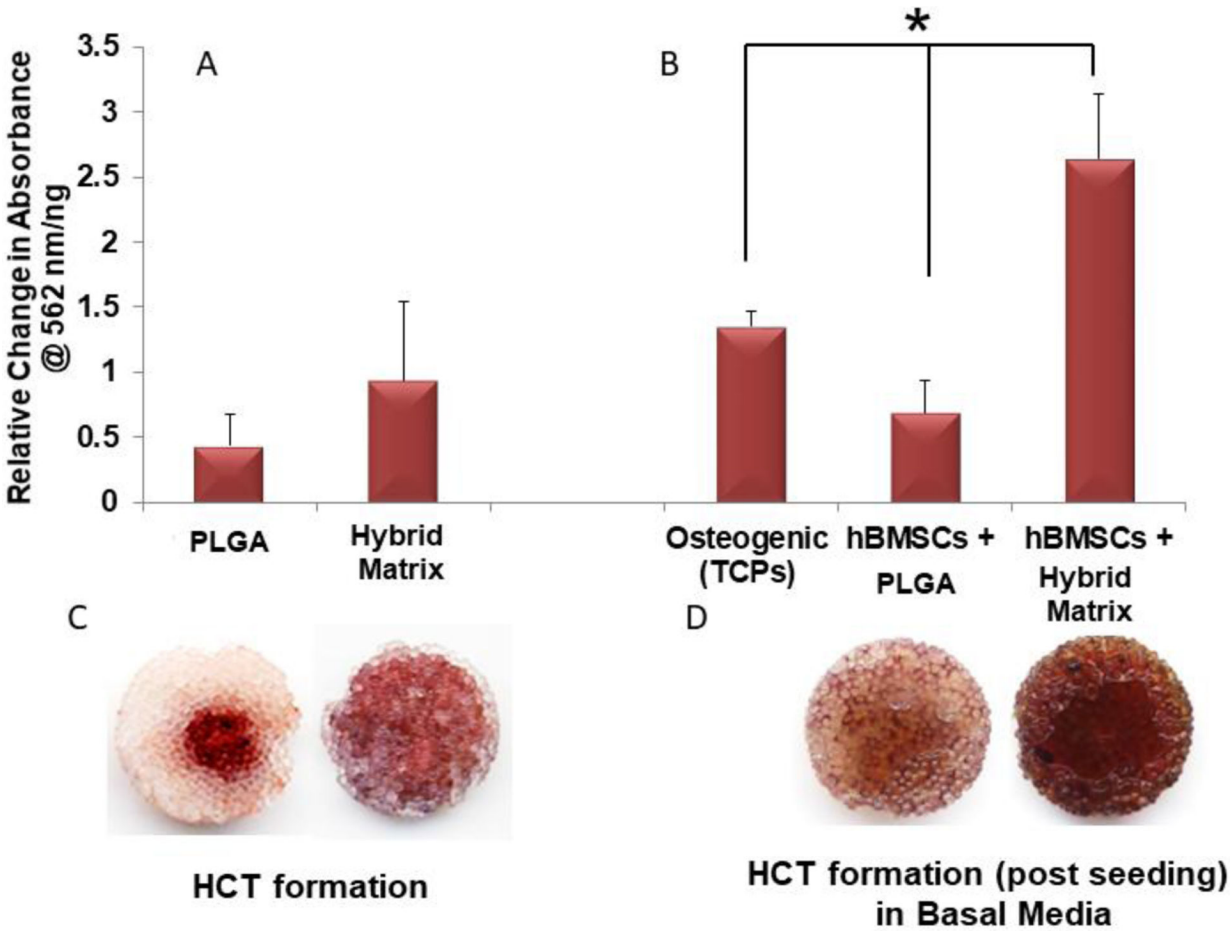

Figure 5.

Hypertrophic cartilage template induced mineralization: Extracellular calcium deposition on PLGA and hybrid matrices before (A) and after homing (B). Both scaffolds and fresh hBMSCs are added to ultra-low attachment plates and cultured in basal media for 21 days to evaluate cell homing and subsequent extracellular calcium deposition ($n=3$, $p<0.05$). Representative images of alizarin red stained PLGA (left) and hybrid (right) matrices before (C) and after (D) fresh hBMSCs seeding.

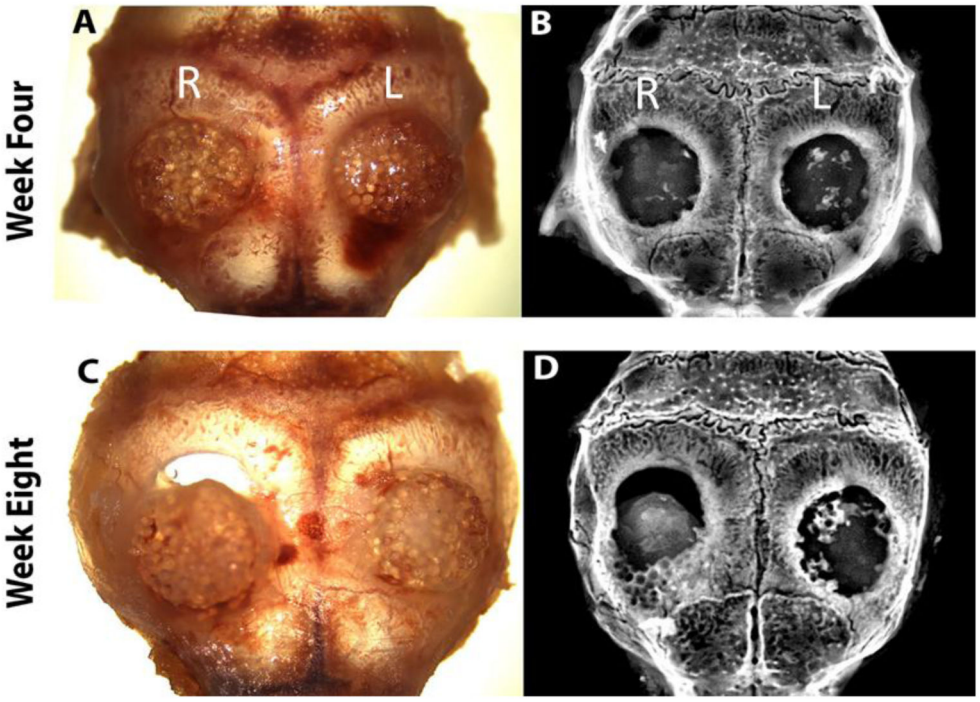

Figure 6.

Matrix implantation in a mice calvarial defect model: At week 4 and 8, animals were scarified and calvarial samples were harvested: top panel four weeks (A) digital photograph and (B) X-ray image. Bottom panel eight weeks (C) digital photograph and (D) X-ray image. (R and L) indicates right side (PLGA matrix) and left side (hybrid matrix) of defect, respectively.

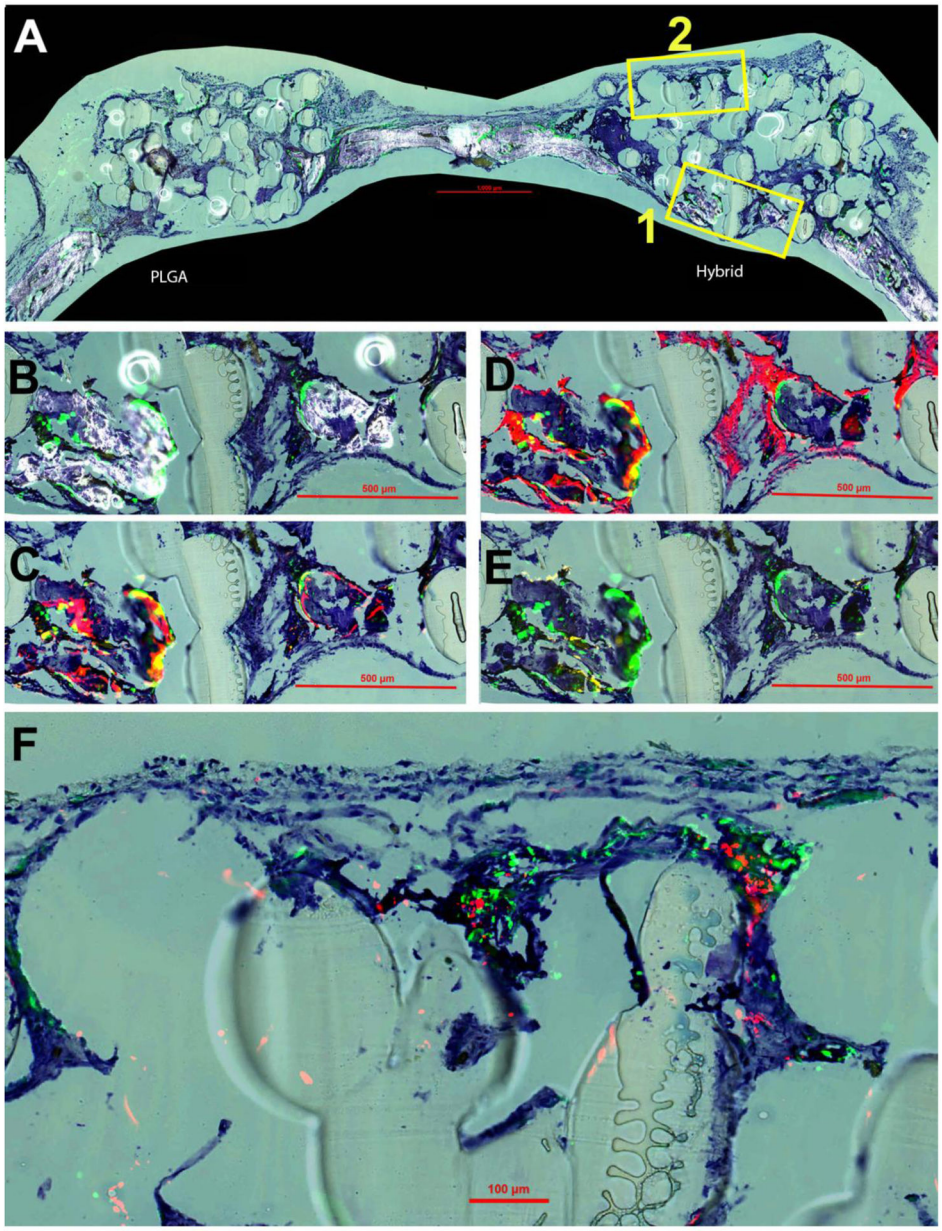

Figure 7.

New bone formation at four weeks post-implantation. Toluidine blue (TB) staining is present in all panels for orientation purposes. (A) Overall representation of entire calavaria for both PLGA and hybrid matrices for detection of mineralization (white) and cellular GFP (green) signal. Box 1 is enlarged and shown in panels B-E and Box 2 in panel F. (B) Enlarged view of boxed portion of A for hybrid matrix. (C) Overlay of AC (alizarin complexone) (red) and GFP signal. (D) Overlay of AP (alkaline phosphatase) (also red) and GFP. (E) Overlay of TRAP staining (tartrate resistant acid phosphatase) (yellow) and GFP. (F) High magnification image of overlay of GFP and HuNuc Ag (human nuclear antigen).

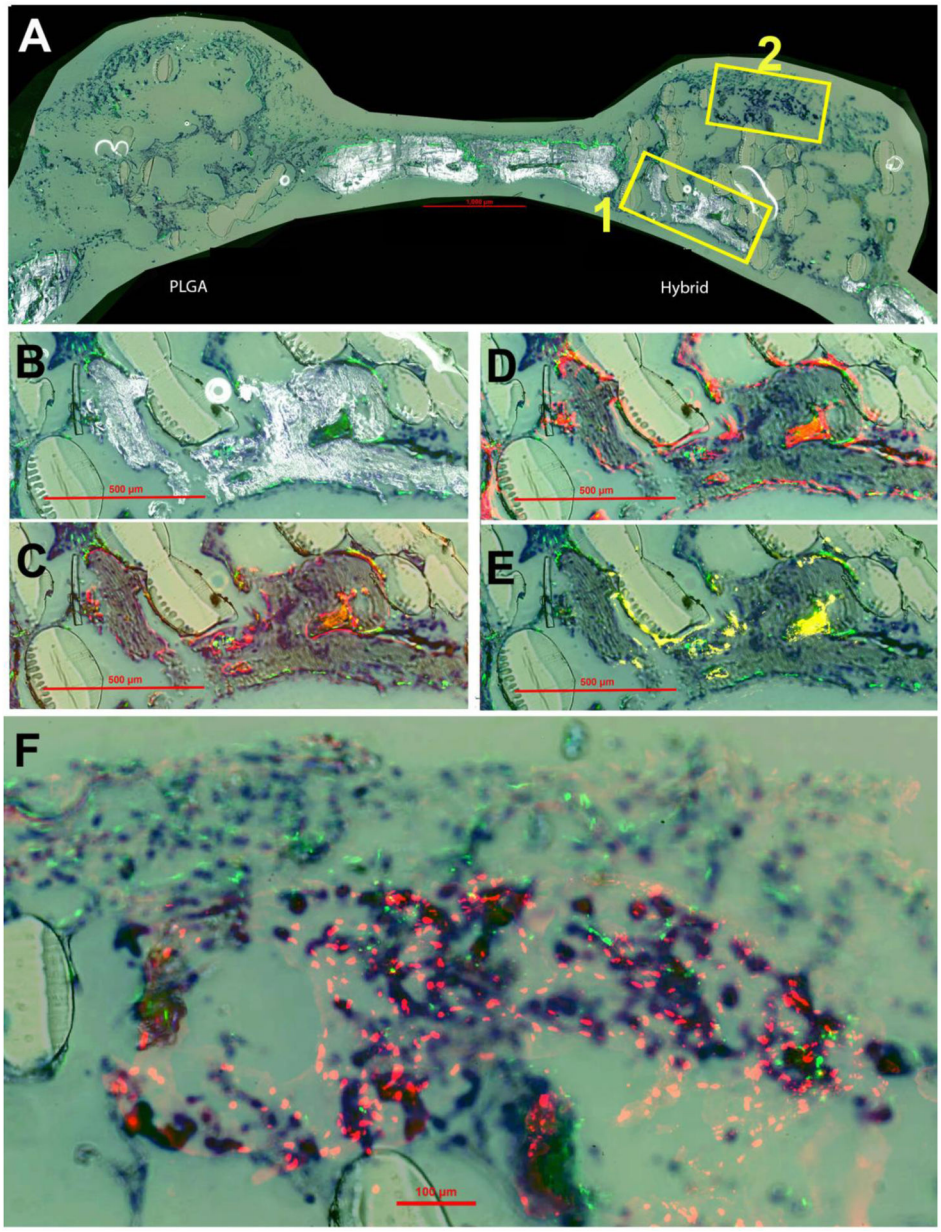

Figure 8.

New bone formation at eight weeks post-implantation. Toluidine blue (TB) staining is present in all panels for orientation purposes. (A) Overall representation of entire calavarial model for both PLGA and hybrid matrices by overlay of mineralization and GFP (green host cells) signal. Box 1 is enlarged and shown in panels B-E and Box 2 in panel F. (B) Enlarged view of boxed portion of A for hybrid matrix. (C) Overlay of AC (alizarin complexone) (red) and GFP signal. (D) Overlay of AP (alkaline phosphatase) (also red) and GFP. (E) Overlay of TRAP staining (tartrate resistant acid phosphatase) (yellow) and GFP. (F) High magnification image of overlay of GFP and HuNuc Ag (human nuclear antigen) (red donor cells).